Published in final edited form as:
Oncogene. 2022 January 01; 41(4): 476–488. doi:10.1038/s41388-021-02080-1.

CHK1 inhibition exacerbates replication stress induced by IGF blockade

Xiaoning Wu[1], **Elena Seraia**[2], **Stephanie B. Hatch**[2], **Xiao Wan**[2], **Daniel V. Ebner**[2], **Francesca Aroldi**[1], **Yanyan Jiang**[3], **Anderson J. Ryan**[3], **Thomas Bogenrieder**[4,5,6], **Ulrike Weyer-Czernilofsky**[4], **Dr Guillaume Rieunier**[1,7,*], **Dr Valentine M. Macaulay**[8,*]

[1]Department of Oncology, University of Oxford, Old Road Campus Research Building, Oxford OX3 7DQ, UK

[2]Target Discovery Institute, University of Oxford, Oxford OX3 7FZ UK

[3]CRUK/MRC Oxford Institute for Radiation Oncology, University of Oxford, Old Road Campus Research Building, Oxford, OX3 7DQ, UK

[4]Boehringer Ingelheim RCV GmbH & Co KG, Dr.-Boehringer-Gasse 5-11, 1121 Vienna, Austria

[5]AMAL Therapeutics, c/o Fondation pour Recherches Médicales, 1205 Geneva, Switzerland

[6]Department of Urology, University Hospital Grosshadern, Ludwig-Maximilians-University, Marchioninistrasse 15, 81377 Munich, Germany

[7]Present address: Immunocore Ltd, Park Drive, Milton Park, Abingdon OX14 4RY, UK

[8]Nuffield Department of Surgical Sciences, University of Oxford, Old Road Campus Research Building, Oxford OX3 7DQ, UK

Abstract

We recently reported that genetic or pharmacological inhibition of insulin-like growth factor receptor (IGF-1R) slows DNA replication and induces replication stress by downregulating the regulatory subunit RRM2 of ribonucleotide reductase, perturbing deoxynucleotide triphosphate (dNTP) supply. Aiming to exploit this effect in therapy we performed a compound screen in five breast cancer cell lines with IGF neutralising antibody xentuzumab. Inhibitor of checkpoint kinase CHK1 was identified as a top screen hit. Co-inhibition of IGF and CHK1 caused synergistic suppression of cell viability, cell survival and tumour growth in 2D cell culture, 3D spheroid cultures and *in vivo*. Investigating the mechanism of synthetic lethality, we reveal that CHK1 inhibition in IGF-1R depleted or inhibited cells further downregulated RRM2, reduced

[*]Joint senior and corresponding authors Dr G. Rieunier: guillaume.rieunier@immunocore.com Dr VM Macaulay: valentine.macaulay@nds.ox.ac.uk .

Author Contributions

XW, GR and VMM designed the study and XW performed most of the experiments, with additional data from GR, ES, SBH, DVE and FA. Xentuzumab was provided by UWC and TB, and GR, YJ and AJR supervised the design and conduct of *in vivo* experiments. The manuscript was written by XW and VMM and reviewed by all co-authors.

Competing interest statement: VMM is a consultancy board member for Boehringer Ingelheim, TB is an employee and UWC an ex-employee of Boehringer Ingelheim. The other authors have declared that there is no conflict of interest.

Europe PMC Funders Author Manuscripts

dNTP supply and profoundly delayed replication fork progression. These effects resulted in significant accumulation of unreplicated single-stranded DNA and increased cell death, indicative of replication catastrophe. Similar phenotypes were induced by IGF:WEE1 co-inhibition, also via exacerbation of RRM2 downregulation. Exogenous RRM2 expression rescued hallmarks of replication stress induced by co-inhibiting IGF with CHK1 or WEE1, identifying RRM2 as a critical target of the functional IGF:CHK1 and IGF:WEE1 interactions. These data identify novel therapeutic vulnerabilities and may inform future trials of IGF inhibitory drugs.

Introduction

Many cancers show aberrant signaling via the insulin-like growth factor (IGF) axis, activating type 1 IGF receptors (IGF-1Rs) and variant insulin receptors (INSRs) to signal via phosphatidylinositol 3-kinase–AKT–mammalian target of rapamycin (PI3K-AKT-mTOR) and mitogen-activated protein kinase kinase–extracellular signal-regulated kinases (MEK-ERK) (1). Through these effectors, IGFs mediate cell cycle progression, cancer cell proliferation and protection from apoptosis (1–3). Previous studies from our group and others revealed that IGF-1R blockade sensitises human tumour cells to ionising radiation (IR) and cytotoxic drugs (4–9). We further reported that IGF-1R depletion or inhibition delays repair of IR-induced DNA double-strand breaks (DSBs), and inhibits DSB repair via both homologous recombination (HR) and non-homologous end-joining (5, 6).

The present study was underpinned by three observations. First, given evidence that IGFs regulate the response to IR, we also found evidence that IGF-1R depletion induced endogenous DNA lesions marked by γH2AX foci in prostate cancer cells (10). The origin of these lesions was unclear, although γH2AX foci are known to accumulate at DSBs and stalled replication forks to recruit repair and cell signalling machineries, serving as a sensitive indicator of DNA damage and replication stress (11, 12). Secondly, we noted that an IGF gene signature identified in MCF7 breast cancer cells included components of the replication machinery (13). Thirdly, we recently identified an absolute requirement for IGF-1 to maintain replication integrity by regulating the function of ribonucleotide reductase (14), the rate-limiting step for dNTP production (15). RNR contains two subunits: ribonucleotide reductase subunit M1 (RRM1) and M2 (RRM2) (16). Acting via both PI3K-AKT and MEK-ERK-JUN pathways, we showed that IGF-1 potently upregulates RRM2 transcription (14). Thus, IGF-1R inhibited or depleted cells downregulate RRM2 and dNTP supply, delaying replication fork progression, activating ATR/CHK1 and the replication checkpoint, and suppressing new origin firing (14), all key hallmarks of replication stress (17). The resulting single-stranded DNA (ssDNA) lesions were found to be marked by γH2AX foci and 53BP1 nuclear bodies, which form in G1 phase to protect from erosion under-replicated DNA generated by mitotic transmission of chromosomes under replication stress (18, 19). Finally, we showed that ssDNA lesions are converted to toxic DSBs in cells lacking functional ataxia telangiectasia mutated (ATM), likely due to failure to form 53BP1 bodies and/or a role for ATM in SSB repair or fork protection (14).

While striking, the replication stress phenotype induced by IGF blockade appeared tolerable with minor impact on viability. Hypothesising that this state represents an

Europe PMC Funders Author Manuscripts

exploitable vulnerability, we conducted a compound screen using IGF neutralising antibody xentuzumab, currently undergoing clinical evaluation with evidence of benefit in patients with oestrogen receptor positive (ER+) breast cancer and non-visceral metastases (20–22). We tested 5 ER+ breast cancer cell lines with xentuzumab alone or with a compound library of inhibitors targeting cell cycle controls, replication and repair. Our recent report described screen outcomes in MCF7 cells (14); here we describe the findings in the full cell line panel. We show that tolerable replication stress in IGF-inhibited cells is exacerbated by co-targeting IGF with CHK1 or WEE1 due to profound RRM2 protein depletion, consistent with roles for these checkpoint kinases in maintaining E2F1-mediated RRM2 transcription and counteracting CDK-mediated RRM2 degradation (23–25). This approach represents a potential treatment strategy that induces intolerable replication stress, replication catastrophe and tumour cell death.

Results

IGF axis inhibition induces tolerable replication stress associated with therapeutic vulnerabilities

Using genetic and pharmacological approaches to block IGF signalling, we recently uncovered a previously-unrecognised role for IGFs in regulating global DNA replication, with replication stress upon IGF axis blockade (14). To confirm this effect, we first tested IGF ligand antibody xentuzumab (BI-836845), and IGF-1R tyrosine kinase inhibitor BI-885578 (20, 26) in MCF7 breast cancer cells. Both drugs caused dose-dependent inhibition of IGF-induced phosphorylation of IGF-1R, AKT and ERKs (Figure 1A). We observed significant increase in γH2AX foci in xentuzumab-treated MCF7 cells (Figure 1B). The foci were comparable in size and intensity to foci induced by aphidicolin that causes replication stress by inhibiting replicative DNA polymerases (27); some aphidicolin-treated cells also exhibited pan-nuclear γH2AX, suggesting DNA damage-induced apoptosis (28). Accumulating γH2AX foci were also induced by IGF-1R depletion in MCF7 cells (Figure 1C), and by xentuzumab treatment in a second ER+ breast cancer cell line, ZR-75-1 (Supplementary Figure S1A), consistent with our previous findings in prostate and breast cancer cells (10, 14). To investigate this initial evidence of replication stress, we assessed replication fork dynamics. Labelling newly-replicated DNA with 5-chloro-2′deoxyuridine (CIdU) and 5-iodo-2′deoxyuridine (IdU), DNA fiber assays enable quantification of the rate of fork progression, fork stalling and origin firing (29). Significant shortening of DNA tracts was detected in MCF7 cells treated with xentuzumab or BI-885578, and in IGF-1R-depleted cells compared to siControls (Figure 1D-E). There was no evidence of significant fork stalling (only CIdU labelling), increased origin firing (only IdU labelling, ref (29), or sister fork asymmetry (Supplementary Figure S1B-D). The latter finding suggested that replication fork delay was due to global reduction in replication rather than localised DNA lesions (30). When we tested consequences for cell viability, MCF7 cells retained 50-70% viability of controls after exposure to xentuzumab or BI-885578, or IGF-1R depletion (Figure 1F-G). These data confirmed our previous finding of significant but tolerable replication stress in IGF-inhibited or IGF-1R-depleted cells (14).

Aiming to enhance this phenotype to intolerable levels, we performed a compound screen to identify additive or synergistic drug combinations with xentuzumab. We chose to screen luminal ER+ breast cancer cell lines because xentuzumab is undergoing trials in ER+ breast cancer, with evidence of benefit in patients with non-visceral metastases (20–22). MCF7, ZR-75-1, KPL1, T47D, and HCC1143 cell lines were tested against a custom compound library of inhibitors targeting cell signalling, cell cycle control, DNA replication and DNA damage responses (Figure 2A, Supplementary Table S1). Compounds were tested at 0.1 μM, 1 μM and 10 μM in the absence or presence of 1 μM xentuzumab, which is near the steady-state circulating concentration at the dose selected for Phase II trials (21). In initial Incucyte tests we optimised seeding densities and confirmed that xentuzumab caused detectable but relatively minor viability inhibition (Supplementary Figure S2A). For the screens, cells were treated with compounds alone or with xentuzumab, or xentuzumab alone, and cell viability determined after 5 days (Figure 2A). Calculated according to (31), screen Z-factor >0.5 indicates excellent screen quality, Z-factor 0-0.5 acceptable and Z-factor ≤0 inadequate (overlap between positive and negative controls). Using DMSO (solvent) as negative control and PLK inhibitor BI-2536 as positive control, most screens were excellent/acceptable, with Z-factors for MCF7 screens of ≥0.64, for T47D and HCC1143 ≥0.5, for ZR-75-1 0.24, 0.52, 0.65 at 0.1, 1 and 10 μM respectively. KPL1 screens gave Z-factors <0 at 0.1 and 1 μM and 0.48 at 10 μM, so only the latter was used to investigate hits. Compounds were ranked on Z-scores; those with Z-score >2 were identified as positive hits that sensitised to xentuzumab (Figure 2B, Supplementary Tables S2-6). Figure 2C shows the overlap of hits between cell lines, and below, the 6 top-ranked compounds. Screen hits in ≥3 cell lines included inhibitors of ATM but not ATR, confirming data from our recent report (14), and inhibitors of PARP, as reported by others (32). Of the 6 compounds, the only agent not previously reported to be at least additive with IGF axis inhibition was CHK1 inhibitor MK-8776. This was also the only compound to achieve Z-score >3 with xentuzumab when comparing Z-scores of cell cycle/repair proteins CHK1, ATM, ATR and PARP. None of the compounds found to have Z-scores >2 with xentuzumab (Supplementary Table S7A) had Z-score >2 when tested alone in the same cell line (Supplementary Table S7B). MK-8776 was of particular interest having been shown to induce replication stress (23, 33, 34). Therefore, we investigated the hypothesis that CHK1 has a protective role in the context of IGF inhibition.

MK-8776 was a screen hit in T47D, KPL1 and HCC1143 but not MCF7 or ZR-75-1 (Supplementary Tables S2-6). However, these may have been false negatives: viability and clonogenic assays in MCF7 and ZR-75-1 showed evidence of a combination effect between MK-8776 and xentuzumab or IGF-1R depletion (Figure 2D-E, Supplementary Figure S2B-C). A similar combination effect was observed in KPL1 cells co-treated with MK-8776 and xentuzumab, confirming MK-8776 as a screen hit in this cell line, and HeLa cervical cancer cells (Supplementary Figure S2D-E). MCF7 cells were also sensitised by BI-885578 to MK-8776 (Figure S2F), and by xentuzumab to alternative CHK1 inhibitors LY2603618 and UCN-01 (Figure 2F-G). These results using inhibitors of different classes provide support for functional interaction between CHK1 and IGF axis inhibition.

CHK1 inhibition induces replication catastrophe in IGF-1R depleted cells

The ATR/CHK1 pathway plays a critical role in mediating replication stress responses during S phase (23, 35, 36). We hypothesized that targeting CHK1 would exacerbate replication stress and viability inhibition induced by IGF blockade. In DNA fiber assays DNA fiber tract shortening was induced by MK-8776 or IGF-1R depletion, the latter effect consistent with Figure 1E, and MK-8776 caused highly significant fiber shortening in IGF-1R depleted cells (Figure 3A), indicating extreme replication fork delay. ATR-CHK1 inhibition is reported to induce unscheduled origin firing (37), and indeed, MK-8776 promoted origin firing in MCF7 cells (Supplementary Figure S3A). Given the reported ability of ATM loss to sensitise to ATR/CHK1 inhibition (38), and our recent finding that ATM loss synergises with IGF axis inhibition (14), we also tested ATM-deficient SK-CO-1 colorectal cancer (CRC) cells (39). Here, MK-8776 or IGF-1R depletion caused replication fork delay, while the combination induced dramatic suppression of fork progression without additive effect on new origin firing (Supplementary Figure S3B). We also performed fiber assays in MCF7 cells after 24 h exposure to MK-8776, xentuzumab or BI-885578. Separately, each agent caused significant replication delay, and MK-8776 increased newly-fired origins, while addition of xentuzumab or BI-885578 to MK-8776 resulted in much shorter DNA fibers (Supplementary Figure S3C-D).

These data suggested that IGF:CHK1 co-inhibition dramatically suppressed DNA replication. This effect was associated with significant increase in non-replicating S-phase cells, those with DNA content between 2N and 4N without incorporation of 5-Bromo-2'-deoxyuridine (BrdU), in IGF-1R depleted MK-8776-treated cells (Figure 3B). To determine whether these treatments had induced polyploidy, which could cause the apparent increase in BrdU-negative cells with DNA content between 2N and 4N, we also checked ungated data. After IGF-1R depletion alone there were fewer than 1% polyploid cells, with no increase upon addition of MK-8776 (Supplementary Figure S3E). This suggests that there was a genuine increase in non-replicating S-phase cells, and that S-phase transit was indeed severely compromised. We then performed double immunostaining assays for two replication stress consequences: γH2AX and ssDNA, the latter visualized by BrdU labelling and detection under non-denaturing conditions (23). Focal and pan-nuclear γH2AX are established markers of replication stress-induced strand breaks and apoptosis (11, 28, 40). Quantifying γH2AX-positive cells as those with >10 foci or pan-nuclear staining as (11), MK-8776 treatment of siControl transfectants enhanced focal and pan-nuclear γH2AX signal (Figure 3C), consistent with previously reported results upon UCN-01 treatment (41), with significant increase upon IGF-1R depletion (Figure 3C upper graph). Native BrdU staining (ssDNA) was also significantly increased by this combination (Figure 3C middle). Quantifying cells double positive for γH2AX and BrdU revealed evidence of a greater than additive effect upon MK-8776 treatment of IGF-1R depleted cells (Figure 3C, lower), consistent with high levels of replication stress and replication catastrophe (23, 35). Investigating the consequences of this phenotype, we quantified cell death using Hoechst 33342, which stains both live and dead cells, and propidium iodide (PI) that binds DNA only in dead cells (42). IGF-1R depletion or 1 μM xentuzumab induced death of <10% MCF7 cells, whereas 1 μM BI-885578 caused 27 ± 1.22% cell death (Figure 3D-E), possibly reflecting more potent IGF-1R inhibition (Figure 1A) and/or additional INSR inhibition

(26). Cell death was significantly increased by addition of MK-8776 in IGF-1R depleted cells and cells treated with xentuzumab or BI-885578 (Figure 3D-E). Together, these data strongly suggest that CHK1 inhibition enhanced replication stress induced by IGF blockade to intolerable levels, triggering replication catastrophe and cell death.

CHK1 inhibition exacerbates RRM2 downregulation and dNTP pool reduction induced by IGF-1R depletion, with rescue by RRM2 overexpression

Given our finding that IGF-1R blockade causes transcriptional RRM2 downregulation (14), and reports that ATR/CHK1 inhibition downregulates RRM2 protein (23, 24), we assessed effects of IGF:CHK1 co-targeting on RRM2. Treating MCF7 cells with MK-8776 after siRNA transfection, we found that MK-8776 suppressed CHK1 autophosphorylation on S296, which targets CDC25 phosphatases to arrest cell cycle progression (43), verifying MK-8776 bioactivity, and increased S345-CHK1 phosphorylation (Figure 4A). The latter effect is likely a feedback consequence of CHK1 inhibition, which deregulates CDK activity leading to increased origin firing, nucleotide depletion and fork breakage, triggering ATR activation (41). MK-8776 or IGF-1R depletion caused moderate RRM2 protein reduction, with further reduction when these treatments were combined (Figure 4A). RRM2 is a key component of the RNR complex, required to convert NDPs into dNDPs (16). Therefore, we next investigated effects on dNTP content, having previously found in HLPC-based assay of MCF7 cell extracts that IGF-1R depletion reduced dATP with no change in dTTP or dGTP, and dCTP was undetectable (14). Here, we modified an alternative assay (44) based on incorporation of tritium-labelled dNTPs into template DNA, using commercially-sourced dNTPs as controls (Supplementary Figure S4A-D). All dNTPs were detectable in MCF7 extracts, and consistent with our previous results (14) IGF-1R depletion reduced only dATP (Figure 4B). Combining MK-8776 and IGF-1R depletion further suppressed dNTP availability with significant reduction in dATP, dTTP and dCTP (Figure 4B), although the changes were relatively modest.

To assess the association of these phenotypes with RRM2 downregulation we generated MCF7 cells stably expressing empty vector (EV) or RRM2. IGF-1R depletion reduced RRM2 protein in EV controls (Figure 4C) as in parental MCF7 (Figure 4A), and also in RRM2-overexpressing cells likely due to downregulation of endogenous RRM2, although residual RRM2 still exceeded levels in siControl-transfected EV controls (Figure 4C). As before (Figure 4A), MK-8776 blocked phospho-S296 CHK1 and increased phospho-S345 CHK1. In EV controls RRM2 was profoundly reduced by combining MK-8776 with IGF-1R depletion, comparable to the effect in parental MCF7 cells (Figure 4A), while RRM2-overexpressing cells maintained RRM2 levels after CHK1 inhibition and IGF-1R depletion (Figure 4C). Testing consequences for cell viability, IGF-1R depletion shifted the MK-8776 dose-response curve to the left in EV controls (Figure 4D), again consistent with results in parental cells (Figure 2C), while RRM2 overexpression shifted the curve to the right, with MK-8776 GI_{50} values >10 μM (Figure 4D). IGF-1R depletion profoundly sensitised EV cells to MK-8776 but had no effect in RRM2-overexpressing cells, with GI_{50} remaining >10 μM (Figure 4D). Similar results were observed on testing xentuzumab with MK-8776: in EV controls, xentuzumab reduced the MK-8776 GI_{50} from >10 μM to 3.8 μM, with a much smaller change (GI_{50} reduced from >10 to 9.6 μM) upon RRM2 overexpression

(Figure 4E). These data indicate almost complete rescue from suppression of cell viability upon IGF:CHK1 co-inhibition.

We next investigated whether RRM2 overexpression influenced replication fork progression. In EV controls, MK-8776 or IGF-1R depletion alone caused moderate fiber shortening, while the combination caused extreme shortening (Figure 5A) consistent with effects in parental MCF7 (Figure 3A). In RRM2-overexpressing cells, DNA fiber tracts were significantly longer than EV controls upon IGF-1R depletion and MK-8776 treatment alone or in combination (Figure 5A). This suggests that RRM2 overexpression rescued replication fork progression, although the rescue effect was partial: in RRM2-overexpressing cells mean fiber length upon combination treat was still shorter than in solvent-treated controls (Figure 5A). RRM2 overexpression did not affect MK-8776-induced aberrant origin firing (Supplementary Figure S5A) but rescued completely from accumulation of non-replicating S-phase cells in MK-8776-treated, IGF-1R depleted cells (Supplementary Figure S4B). We observed significant rescue from replication catastrophe, with fewer cells double-positive for γH2AX and ssDNA following MK-8776 treatment and IGF-1R depletion (Figure 5B). This co-treatment also induced significantly less cell death in RRM2-overexpressing cells compared with EV controls (Figure 5C). Thus, RRM2 overexpression restored RRM2 protein, alleviated replication stress and rescued from cell death, suggesting that RRM2 is an important target of the interaction between CHK1 inhibition and IGF blockade.

IGF-inhibited cells are sensitive to CHK1 inhibition in anchorage-independent growth

Cancer cell spheroids recapitulate features of tumour growth *in vivo*, including increased cell-cell interactions and normoxic, hypoxic and necrotic zones reflecting tumour complexity (45–47). MCF7 spheroids grew very slowly (~1.5-fold increase over 6 days) with no suppression by xentuzumab, partial inhibition by MK-8776, and a combination effect with xentuzumab at only 3 μM MK-8776 (Supplementary Figure S6A). We examined alternative models as a preliminary to *in vivo* testing, and found that SK-CO-1 spheroids were sensitive to xentuzumab, consistent with our *in vivo* data (14), and were also inhibited by 3 μM MK-8776 alone (Figure 6A-B). There was further growth inhibition in the presence of xentuzumab plus 3 μM MK-8776, with significant spheroid size regression and reduction in spheroid viability (Figure 6B-C). HeLa spheroids were growth delayed by 1 μM xentuzumab or 3 or 10 μM MK-8776, showed almost complete growth arrest with the xentuzumab/MK-8776 combination, and a similar combination effect in response to BI-885578 plus MK-8776 (Supplementary Figure S6B-C). We then tested another highly selective CHK1 inhibitor, SRA737 (48), which dose-dependently suppressed SK-CO-1 spheroid growth, with further significant suppression with 1 μM xentuzumab, including regression in the presence of 10 μM SRA737 and xentuzumab (Supplementary Figure S6D). SRA737 also reduced cell viability in SK-CO-1 spheroids, with further reduction upon addition of 1 μM xentuzumab (Supplementary Figure S5E). HeLa spheroid viability was largely unaffected by 1 μM xentuzumab or MK-8776 alone but showed a combination effect upon co-treatment of xentuzumab with 3 or 10 μM MK-8776 or 3 μM SRA737 (Supplementary Figure S5F-G). Having previously reported that IGF targeting affects DNA damage responses in prostate cancer cells (6, 10), we also tested xentuzumab and MK-8776

in 22Rv1 prostate cancer spheroids, again finding a combination effect of this co-treatment on spheroid growth and viability (Supplementary Figure S6H).

Given the sensitivity of SK-CO-1 spheroids to IGF:CHK1 co-inhibition (Figure 6A-B), we tested xentuzumab and MK-8776 in mice bearing SK-CO-1 xenografts. *In vivo*, MK-8776 was administered in (2-Hydroxypropyl)-beta-cyclodextrin, as had been used in previous *in vivo* assessment of this drug (49, 50). However, on starting treatment, tumour growth slowed even in controls treated with (2-Hydroxypropyl)-beta-cyclodextrin, which was previously reported to inhibit growth and enhance apoptosis (51). Following 18 days treatment, combination-treated tumours were significantly smaller than the control and MK-8776 groups but not the xentuzumab alone group (Supplementary Figure S6I, left). Off treatment, we observed regrowth of tumours in all groups except the combination treatment group, where mean tumour size was 23 ± 4% of controls, but the differences were not significant (Supplementary Figure S6I, right). As an alternative route to assess combination effects we calculated Combination Indices (CI) from SK-CO-1 spheroid viability data using the Chou-Talalay method (52). All combinations except the lowest concentrations (100 nM xentuzumab, 0.3 μM MK-8776) yielded CI values <0.8, with some values 0.1-0.3 indicating strong synergy between co-inhibition of IGF and CHK1 (Figure 6D). We also tested for combination effects using Bliss Independence (53), expressing the results as predicted/observed fraction affected. All but one of the combinations generated values of <0.8, supporting a synergistic relationship between xentuzumab and MK-8776 (Supplementary Table S8).

To probe the mechanism of synergy we assessed RRM2 and dNTP levels in SK-CO-1 spheroids following 7 days treatment with xentuzumab and MK-8776 (Figure 6A). In western blots of spheroid extracts, xentuzumab abolished ~98 kDa phospho-IGF-1R signal but induced 90-95 kDa signal, possibly phospho-INSR. RRM2 was largely unaffected by xentuzumab or MK-8776 alone but was significantly downregulated by combination treatment (Figure 6E-F). In dNTP assays, given very small amounts of material, only dATP was detectable in SK-CO-1 spheroids, and was markedly reduced by the MK-8776 plus xentuzumab combination (Figure 6G). It would have been advantageous to confirm these results in HeLa spheroids given the effect of this drug combination on spheroid growth (Supplementary Figure S6B), but their smaller size prevented us from assaying dNTPs or other markers. None-the-less, the results in SK-CO-1 spheroids support our hypothesis that IGF:CHK1 co-targeting compromises dNTP supply.

WEE1 inhibition induces replication catastrophe in IGF-1R depleted cells via RRM2 downregulation

Given our finding that IGF:CHK1 co-inhibition downregulates RRM2 inducing severe replication stress, we considered whether a similar response to IGF blockade is achieved by other compounds that influence RRM2. In our screen, the inhibitor of cell cycle checkpoint kinase WEE1, MK-1775, sensitised to xentuzumab only in KPL1 cells (Supplementary Tables S2-6). In MCF7 cells, MK-1775 blocked inhibitory Tyr-15 CDK1 phosphorylation and reduced RRM2 protein, consistent with (25), and induced ATR-mediated phospho-S345 CHK1 phosphorylation (Figure 7A), suggesting replication stress. IGF depletion

increased phospho-Tyr15 CDK1, not reported previously, suggesting WEE1 activation after IGF blockade. Notably, IGF-1R depletion plus MK-1775 resulted in further RRM2 downregulation (Figure 7A), suppressed cell viability and induced excess cell death compared to siControls (Figure 7B-C). Xentuzumab or BI-885578 also significantly sensitised MCF7 cells to MK-1775 in viability and clonogenic assays (Supplementary Figure S7A-C). This suggests that MK-1775 was a false negative in the MCF7 screen, although the effect on response to MK-1775 was less marked than the sensitisation induced by xentuzumab to MK-8776 (Figure 2D, Supplementary Figure S2B). MK-1775 also markedly suppressed SK-CO-1 spheroid growth (Supplementary Figure S7D), supporting a combination effect of co-inhibiting IGF and WEE1.

Consistent with effects on RRM2 protein, the combination of MK-1775 and IGF-1R depletion caused major replication tract delay, accumulation of cells in non-replicating S-phase and cells double-positive for γH2AX and ssDNA (Figure 7D-F). Collectively, these results suggest that WEE1 inhibition exacerbated replication stress caused by IGF blockade, inducing replication catastrophe. To confirm the role of RRM2 downregulation in inducing these phenotypes, it would be advantageous to test for rescue by RRM2 overexpression. However, we did test effects of RRM2 overexpression on viability: comparable to data generated using MK-8776 (Figure 4D-E), RRM2 overexpression rescued almost completely from the inhibitory effect on cell viability of the combination of MK-1775 with IGF-1R depletion or xentuzumab (Figure 7G-H).

Discussion

Here, we follow up our recent identification of a role for IGFs in regulating DNA replication (14) with approaches to exploit this effect in therapy. We confirm that IGF-1R depletion or IGF inhibition delayed replication fork progression, with accumulation of ssDNA lesions, non-replicating S-phase cells and ATR-CHK1 activation. This was a striking replication stress phenotype, but the effect was largely tolerable. In our previous report, we identified ATM loss as synergistic with IGF inhibition due to conversion of tolerable ssDNA lesions into toxic DSBs (14). The current data identify a different mechanism of synergy, which we show is due to exacerbation of RRM2 downregulation by co-inhibition of CHK1 or WEE1, the IGF-CHK1 inhibitor combination being more effective. We previously reported that response to IGF-1R inhibition was enhanced by suppressing HR in prostate cancer models (10). Here, we find no evidence that sensitivity to IGF:CHK1 co-inhibition associates with HR status, given our detection of combination effects in HR proficient MCF7, T47D, ZR-75-1, HCC1143 and HeLa cells (54–56), and SK-CO-1 and 22Rv1 that are HR deficient judging by PARP inhibitor sensitivity (39, 57). Testing cell lines of different genotypes including immortalised, non-transformed cells, would be necessary to confirm this. CHK1 regulates RRM2 at the transcriptional level via E2F1, and both CHK1 and WEE1 inactivate CDKs, preventing RRM2 being targeted for proteasomal degradation, thus playing an important role in maintaining dNTP pools (23–25, 58).

Given these roles for ATM and CHK1, and evidence of ATR-CHK1 activation in replication-stressed cells, we had predicted that ATR inhibition would also synergise with IGF blockade. Others have reported additive-to-synergistic relationships between ATR inhibition

and IGF-1R inhibitors BMS-754807 (CI values ≥0.777) and OSI-906 (CI ≥0.818) in MCF7 cells, with a stronger effect (CI ≥0.50) in cells induced to be BMS-754807 resistant (59). We previously found no additivity/synergy between xentuzumab and ATR inhibition in MCF7 (14), and confirm here that ATR inhibition was not a hit in any of the 5 screened breast cancer cell lines, while in contrast we find evidence of synergy with CHK1 inhibition. This apparent paradox could relate to data showing or implying that ATR and CHK1 may not always function in tandem, including a report of dissociated ATR:CHK1 function in the context of UV-induced replication stress, synthetic lethality between CHK1 inhibition and ATR inhibition, also suggesting differential function, and identification of an apparently ATR-independent function for CHK1 related to bypass of replication barriers (60–62). Of relevance here, ATR inhibition is reported to induce moderate ssDNA in most S-phase cells. This triggers a DNA-PK/CHK1-mediated backup pathway to suppress origin firing, creating a threshold such that ATR inhibition selectively kills cells under high replication stress, and CHK1 inhibition at a lower threshold (23).

We confirmed the central role of RRM2 in the synthetic lethality of IGF:CHK1 and IGF:WEE1 co-inhibition in an RRM2 overexpression model. Expression of constitutive RRM2 rescued from the major hallmarks of replication stress, including slowing of the replication fork, accumulation of ssDNA and non-replicating S-phase cells, and also prevented replication catastrophe. These data support the hypothesis that IGF-1, like CHK1 and WEE1, plays a key role in RRM2 regulation (Figure 7I). IGF axis inhibitor trials have been compromised by lack of predictive biomarkers, although many trials included patients who obtained benefit, prompting intense efforts to characterise sensitive tumours and design rational drug combinations. Our data reveal CHK1 as a potential partner for co-inhibition with IGF blockade; we suggest that the efficacy of this combination may be most appropriately tested in ATM null tumours given our recent identification of ATM loss as a candidate biomarker for sensitivity to IGF axis blockade (14). CHK1 inhibitors including SRA737 are being tested clinically (63, 64), suggesting that there may be merit in evaluating these agents with IGF axis blockade.

In summary, we highlight the critical role of IGF signaling in mediating DNA replication by regulating RRM2 and dNTP supply, and show that IGF-inhibited cells exhibit tolerable replication stress that represents a therapeutic vulnerability. We identify approaches to exploit this effect by co-inhibiting checkpoint kinases CHK1 or WEE1 to induce cancer cell death through replication catastrophe.

Materials and Methods

Cell lines and reagents

MCF7, ZR-75-1, T47D, and HCC1143 breast cancer cell lines were from Dr Anthony Kong, King’s College London. RRM2-overexpressing MCF7 cells were generated as described (14). HeLa cells were from Professor Adrian Harris, University of Oxford, 22Rv1 from Professor Sir Walter Bodmer, University of Oxford, KPL1 cells were purchased from European Collection of Authenticated Cell Cultures and SK-CO-1 from American Type Culture Collection. Cell lines were negative for mycoplasma infection (MycoAlert, Lonza) and were authenticated by STR genotyping at Cancer Research UK Clare Hall Laboratories

and Eurofins. Early passage stocks were expanded and cryopreserved and used within 20 passages of recovery. Xentuzumab and BI-885578 were obtained from Boehringer Ingelheim. MK-8776, SRA737 and LY2603618 were purchased from Selleck Chemicals, UCN-01 from Cambridge Bioscience, MK-1775 from Axon Medchem and aphidicolin from Sigma-Aldrich.

Viability, death and clonogenic assays were performed as described (6, 14). Viability data were analysed in Graphpad Prism 8 to calculate half-maximal inhibitory concentrations (IC_{50}).

Compound screens were performed in duplicate using a 60-compound custom library (Supplementary Table S1) at 0.1 μM, 1 μM, 10 μM alone or with PBS (control) or 1 μM xentuzumab for 5 days. Cell seeding, treatment and viability assay were as (14). Z-factors (screen quality) and Z-scores (compound ranking) were calculated as described (31, 65) and Supplementary Methods.

Gene silencing, western blot, flow cytometry, DNA fiber assays were performed as (14) using AllStars Negative Control siRNA, IGF-1R siRNA #1 (S100017521) and #2 designed in-house (66), all from Qiagen, and antibodies listed in Supplementary Table S9.

Immunofluorescence for γH2AX and ssDNA: as described in (23) ssDNA was detected by BrdU staining under non-denaturing conditions. Cells were pulsed with 10 μM BrdU (Sigma-Aldrich) and 36 h later fixed with 4% paraformaldehyde for 12 minutes, permeabilized using TFT buffer (0.1% Triton X-100, 4% FBS in phosphate-buffered saline, PBS) for 5 minutes and blocked with 5% BSA in PBS for 1 h. Cells were stained overnight at 4°C with antibodies to BrdU (#347580, BD Biosciences) and γH2AX (# 2577, Cell Signaling Technology) and bound antibodies were detected with anti-mouse antibody Alexa Fluor 488 (#A11029, Invitrogen) and anti-rabbit antibody Alexa Fluor 594 (#A11037, Invitrogen). After mounting with antifade mounting medium containing DAPI (Vector Laboratories), slides were imaged on a ZEISS LSM 710 confocal microscope (Carl Zeiss Microscopy).

dNTP assay utilised a solid-phase polymerase assay modified from (44), using tritium (^3H)-labelled substrates with commercially available dNTPs as standards, as detailed in Supplementary Methods and Supplementary Table S10.

3D spheroid culture was performed as (14). After completing drug treatments, spheroids were used for western blot, dNTP assay or viability assay (CellTiter Glo 3D, Promega). For western blots, ≥3 spheroids for each condition were lysed in 3x Laemmli sample buffer (150 mM Tris-HCl pH 6.8, 0.3 mg/mL Bromophenol blue, 30% Glycerol, 9% SDS, 15% β-mercaptoethanol). For dNTP measurement, twelve spheroids per condition were extracted in 1 mL cold (-20°C) 60% methanol, vigorously vortexed or sonicated at 4°C (Bioruptor sonicator, Diagenode), incubated at –80°C overnight and assayed as described in Supplementary Methods. Samples were normalised using CellTiter Glo 3D or BCA protein assay data to adjust volumes of each extract used for dNTP assay.

In vivo experiments

Animal procedures were conducted under PPL 30/3395 and PIL IC38C8060 issued by the UK Home Office. Before Home Office submission, the Project Licence was approved by the Oxford University Animal Welfare and Ethical Review Board. As described in (14), SK-CO-1 cells ($8x10^6$ cells/mouse) were grown as xenografts in 5-6 week old female CD-1 immunodeficient mice (Charles River Laboratories). When tumours attained ~80-100 mm^3, mice were randomly grouped into 4 groups (N=5) for twice weekly intraperitoneal injection: group 1) PBS with 20% (2-Hydroxypropyl)-beta-cyclodextrin (Sigma-Aldrich); 2) PBS with 50 mg/kg MK-8776 diluted in 20% (2-Hydroxypropyl)-beta-cyclodextrin; 3) 100 mg/kg xentuzumab with 20% (2-Hydroxypropyl)-beta-cyclodextrin; 4) 100 mg/kg xentuzumab with 50 mg/kg MK-8776 in 20% (2-Hydroxypropyl)-beta-cyclodextrin. Mice were monitored regularly, tumours were measured every 2-3 days by Biomedical Services staff who were blinded to treatment allocation, and tumour volumes calculated as Volume (mm^3) = π/6 x Length (mm) x width (mm) x height (mm).

Statistics

Data were presented as mean ± standard error of mean (SEM), n=3 independent experiments unless stated otherwise. In Graphpad Prism 8 we used two-tailed t-test to compare two groups, one-way analysis of variance (ANOVA) for >2 groups and two-way ANOVA for proliferation, cell death and clonogenic assay dose-response curves, with post-hoc analysis and correction for multiple comparisons to assess significance at each drug concentration. P values <0.05 were considered statistically significant. Combination indices were calculated using CalcuSyn Software (52) and Bliss Independence (53).

Supplementary Material

Refer to Web version on PubMed Central for supplementary material.

Acknowledgements

We acknowledge the assistance and expertise provided by Rhodri Wilson and Graham Brown from the Microscopy core facility, Department of Oncology, University of Oxford. We thank Dr Anthony Kong for MCF7, ZR-75-1, T47D, and HCC1143 breast cancer cell lines, Professor Adrian Harris for HeLa cells and Michael Sanderson (ex-Boehringer Ingelheim, now Merck) for the generous supply of BI-885578. This study was supported by Breast Cancer Now (grant 2014NovPR364 to VMM), Cancer Research UK (grant C476/A27060 to VMM and GR), Oxfordshire Health Services Research Committee (grant 1326 to FA) and support to VMM from the NIHR Oxford Biomedical Research Centre and the Harrington Discovery Institute. We are grateful to Andrew Blackford, Tim Humphrey and Ian Mills for comments on the manuscript.

References

1. Chitnis MM, Yuen JS, Protheroe AS, Pollak M, Macaulay VM. The type 1 insulin-like growth factor receptor pathway. Clin Cancer Res. 2008; 14: 6364–70. [PubMed: 18927274]
2. Borowiec AS, Hague F, Gouilleux-Gruart V, Lassoued K, Ouadid-Ahidouch H. Regulation of IGF-1-dependent cyclin D1 and E expression by hEag1 channels in MCF-7 cells: the critical role of hEag1 channels in G1 phase progression. Biochim Biophys Acta. 2011; 1813: 723–30. [PubMed: 21315112]
3. Hamelers IH, van Schaik RF, Sipkema J, Sussenbach JS, Steenbergh PH. Insulin-like growth factor I triggers nuclear accumulation of cyclin D1 in MCF-7S breast cancer cells. J Biol Chem. 2002; 277: 47645–52. [PubMed: 12364325]

4. Rochester MA, Riedemann J, Hellawell GO, Brewster SF, Macaulay VM. Silencing of the IGF1R gene enhances sensitivity to DNA-damaging agents in both PTEN wild-type and mutant human prostate cancer. Cancer Gene Ther. 2005; 12: 90–100. [PubMed: 15499378]

5. Turney BW, Kerr M, Chitnis MM, Lodhia K, Wang Y, Riedemann J, et al. Depletion of the type 1 IGF receptor delays repair of radiation-induced DNA double strand breaks. Radiother Oncol. 2012; 103: 402–9. [PubMed: 22551565]

6. Chitnis MM, Lodhia KA, Aleksic T, Gao S, Protheroe AS, Macaulay VM. IGF-1R inhibition enhances radiosensitivity and delays double-strand break repair by both non-homologous end-joining and homologous recombination. Oncogene. 2014; 33: 5262–73. [PubMed: 24186206]

7. Cosaceanu D, Budiu RA, Carapancea M, Castro J, Lewensohn R, Dricu A. Ionizing radiation activates IGF-1R triggering a cytoprotective signaling by interfering with Ku-DNA binding and by modulating Ku86 expression via a p38 kinase-dependent mechanism. Oncogene. 2007; 26: 2423–34. [PubMed: 17043647]

8. Ferte C, Loriot Y, Clemenson C, Commo F, Gombos A, Bibault JE, et al. IGF-1R targeting increases the antitumor effects of DNA-damaging agents in SCLC model: an opportunity to increase the efficacy of standard therapy. Mol Cancer Ther. 2013; 12: 1213–22. [PubMed: 23640142]

9. Riesterer O, Yang Q, Raju U, Torres M, Molkentine D, Patel N, et al. Combination of anti-IGF-1R antibody A12 and ionizing radiation in upper respiratory tract cancers. Int J Radiat Oncol Biol Phys. 2011; 79: 1179–87. [PubMed: 21129859]

10. Lodhia KA, Gao S, Aleksic T, Esashi F, Macaulay VM. Suppression of homologous recombination sensitizes human tumor cells to IGF-1R inhibition. Int J Cancer. 2015; 136: 2961–6. [PubMed: 25388513]

11. Gagou ME, Zuazua-Villar P, Meuth M. Enhanced H2AX phosphorylation, DNA replication fork arrest, and cell death in the absence of Chk1. Mol Biol Cell. 2010; 21: 739–52. [PubMed: 20053681]

12. Rogakou EP, Pilch DR, Orr AH, Ivanova VS, Bonner WM. DNA double-stranded breaks induce histone H2AX phosphorylation on serine 139. J Biol Chem. 1998; 273: 5858–68. [PubMed: 9488723]

13. Creighton CJ, Casa A, Lazard Z, Huang S, Tsimelzon A, Hilsenbeck SG, et al. Insulin-like growth factor-I activates gene transcription programs strongly associated with poor breast cancer prognosis. J Clin Oncol. 2008; 26: 4078–85. [PubMed: 18757322]

14. Rieunier G, Wu X, Harris LE, Mills JV, Nandakumar A, Colling L, et al. Targeting IGF perturbs global replication through ribonucleotide reductase dysfunction. Cancer Res. 2021; 81: 2128–41. [PubMed: 33509941]

15. Mathews CK. Deoxyribonucleotide metabolism, mutagenesis and cancer. Nat Rev Cancer. 2015; 15: 528–39. [PubMed: 26299592]

16. Stubbe J, van der Donk WA. Ribonucleotide reductases: radical enzymes with suicidal tendencies. Chem Biol. 1995; 2: 793–801. [PubMed: 8807812]

17. Zeman MK, Cimprich KA. Causes and consequences of replication stress. Nat Cell Biol. 2014; 16: 2–9. [PubMed: 24366029]

18. Harrigan JA, Belotserkovskaya R, Coates J, Dimitrova DS, Polo SE, Bradshaw CR, et al. Replication stress induces 53BP1-containing OPT domains in G1 cells. J Cell Biol. 2011; 193: 97–108. [PubMed: 21444690]

19. Lukas C, Savic V, Bekker-Jensen S, Doil C, Neumann B, Pedersen RS, et al. 53BP1 nuclear bodies form around DNA lesions generated by mitotic transmission of chromosomes under replication stress. Nat Cell Biol. 2011; 13: 243–53. [PubMed: 21317883]

20. Friedbichler K, Hofmann MH, Kroez M, Ostermann E, Lamche HR, Koessl C, et al. Pharmacodynamic and antineoplastic activity of BI 836845, a fully human IGF ligand-neutralizing antibody, and mechanistic rationale for combination with rapamycin. Mol Cancer Ther. 2014; 13: 399–409. [PubMed: 24296829]

21. de Bono J, Lin CC, Chen LT, Corral J, Michalarea V, Rihawi K, et al. Two first-in-human studies of xentuzumab, a humanised insulin-like growth factor (IGF)-neutralising antibody, in patients with advanced solid tumours. Br J Cancer. 2020; 122: 1324–32. [PubMed: 32161368]

22. Schmid P, Sablin MP, Bergh J, Im SA, Lu YS, Martinez N, et al. A phase Ib/II study of xentuzumab, an IGF-neutralising antibody, combined with exemestane and everolimus in hormone receptor-positive, HER2-negative locally advanced/metastatic breast cancer. Breast Cancer Res. 2021; 23: 8. [PubMed: 33451345]

23. Buisson R, Boisvert JL, Benes CH, Zou L. Distinct but Concerted Roles of ATR, DNA-PK, and Chk1 in Countering Replication Stress during S Phase. Mol Cell. 2015; 59: 1011–24. [PubMed: 26365377]

24. Koppenhafer SL, Goss KL, Terry WW, Gordon DJ. Inhibition of the ATR-CHK1 Pathway in Ewing Sarcoma Cells Causes DNA Damage and Apoptosis via the CDK2-Mediated Degradation of RRM2. Mol Cancer Res. 2020; 18: 91–104. [PubMed: 31649026]

25. Pfister SX, Markkanen E, Jiang Y, Sarkar S, Woodcock M, Orlando G, et al. Inhibiting WEE1 Selectively Kills Histone H3K36me3-Deficient Cancers by dNTP Starvation. Cancer Cell. 2015; 28: 557–68. [PubMed: 26602815]

26. Sanderson MP, Apgar J, Garin-Chesa P, Hofmann MH, Kessler D, Quant J, et al. BI 885578, a Novel IGF1R/INSR Tyrosine Kinase Inhibitor with Pharmacokinetic Properties That Dissociate Antitumor Efficacy and Perturbation of Glucose Homeostasis. Mol Cancer Ther. 2015; 14: 2762–72. [PubMed: 26438154]

27. Vesela E, Chroma K, Turi Z, Mistrik M. Common Chemical Inductors of Replication Stress: Focus on Cell-Based Studies. Biomolecules. 2017; 7: 19.

28. Solier S, Sordet O, Kohn KW, Pommier Y. Death receptor-induced activation of the Chk2- and histone H2AX-associated DNA damage response pathways. Mol Cell Biol. 2009; 29: 68–82. [PubMed: 18955500]

29. Merrick CJ, Jackson D, Diffley JF. Visualization of altered replication dynamics after DNA damage in human cells. J Biol Chem. 2004; 279: 20067–75. [PubMed: 14982920]

30. Conti C, Sacca B, Herrick J, Lalou C, Pommier Y, Bensimon A. Replication fork velocities at adjacent replication origins are coordinately modified during DNA replication in human cells. Mol Biol Cell. 2007; 18: 3059–67. [PubMed: 17522385]

31. Zhang JH, Chung TD, Oldenburg KR. A Simple Statistical Parameter for Use in Evaluation and Validation of High Throughput Screening Assays. J Biomol Screen. 1999; 4: 67–73. [PubMed: 10838414]

32. Amin O, Beauchamp MC, Nader PA, Laskov I, Iqbal S, Philip CA, et al. Suppression of Homologous Recombination by insulin-like growth factor-1 inhibition sensitizes cancer cells to PARP inhibitors. BMC Cancer. 2015; 15: 817. [PubMed: 26510816]

33. Dai Y, Chen S, Kmieciak M, Zhou L, Lin H, Pei XY, et al. The novel Chk1 inhibitor MK-8776 sensitizes human leukemia cells to HDAC inhibitors by targeting the intra-S checkpoint and DNA replication and repair. Mol Cancer Ther. 2013; 12: 878–89. [PubMed: 23536721]

34. Parsels LA, Parsels JD, Tanska DM, Maybaum J, Lawrence TS, Morgan MA. The contribution of DNA replication stress marked by high-intensity, pan-nuclear gammaH2AX staining to chemosensitization by CHK1 and WEE1 inhibitors. Cell Cycle. 2018; 17: 1076–86. [PubMed: 29895190]

35. Toledo L, Neelsen KJ, Lukas J. Replication Catastrophe: When a Checkpoint Fails because of Exhaustion. Mol Cell. 2017; 66: 735–49. [PubMed: 28622519]

36. Toledo LI, Altmeyer M, Rask MB, Lukas C, Larsen DH, Povlsen LK, et al. ATR prohibits replication catastrophe by preventing global exhaustion of RPA. Cell. 2013; 155: 1088–103. [PubMed: 24267891]

37. Moiseeva T, Hood B, Schamus S, O'Connor MJ, Conrads TP, Bakkenist CJ. ATR kinase inhibition induces unscheduled origin firing through a Cdc7-dependent association between GINS and And-1. Nat Commun. 2017; 8: 1392. [PubMed: 29123096]

38. Rafiei S, Fitzpatrick K, Liu D, Cai MY, Elmarakeby HA, Park J, et al. ATM Loss Confers Greater Sensitivity to ATR Inhibition than PARP Inhibition in Prostate Cancer. Cancer Res. 2020; 80: 2094–100. [PubMed: 32127357]

39. Wang C, Jette N, Moussienko D, Bebb DG, Lees-Miller SP. ATM-Deficient Colorectal Cancer Cells Are Sensitive to the PARP Inhibitor Olaparib. Transl Oncol. 2017; 10: 190–6. [PubMed: 28182994]

40. Moeglin E, Desplancq D, Conic S, Oulad-Abdelghani M, Stoessel A, Chiper M, et al. Uniform Widespread Nuclear Phosphorylation of Histone H2AX Is an Indicator of Lethal DNA Replication Stress. Cancers (Basel). 2019; 11: 355.
41. Syljuasen RG, Sorensen CS, Hansen LT, Fugger K, Lundin C, Johansson F, et al. Inhibition of human Chk1 causes increased initiation of DNA replication, phosphorylation of ATR targets, and DNA breakage. Mol Cell Biol. 2005; 25: 3553–62. [PubMed: 15831461]
42. Ellwart JW, Dormer P. Vitality measurement using spectrum shift in Hoechst 33342 stained cells. Cytometry. 1990; 11: 239–43. [PubMed: 1690626]
43. Kasahara K, Goto H, Enomoto M, Tomono Y, Kiyono T, Inagaki M. 14-3-3gamma mediates Cdc25A proteolysis to block premature mitotic entry after DNA damage. EMBO J. 2010; 29: 2802–12. [PubMed: 20639859]
44. Landoni JC, Wang L, Suomalainen A. Quantitative solid-phase assay to measure deoxynucleoside triphosphate pools. Biol Methods Protoc. 2018; 3 bpy011 [PubMed: 32161804]
45. Hirschhaeuser F, Menne H, Dittfeld C, West J, Mueller-Klieser W, Kunz-Schughart LA. Multicellular tumor spheroids: an underestimated tool is catching up again. J Biotechnol. 2010; 148: 3–15. [PubMed: 20097238]
46. Nath S, Devi GR. Three-dimensional culture systems in cancer research: Focus on tumor spheroid model. Pharmacol Ther. 2016; 163: 94–108. [PubMed: 27063403]
47. Sant S, Johnston PA. The production of 3D tumor spheroids for cancer drug discovery. Drug Discov Today Technol. 2017; 23: 27–36. [PubMed: 28647083]
48. Booth L, Roberts J, Poklepovic A, Dent P. The CHK1 inhibitor SRA737 synergizes with PARP1 inhibitors to kill carcinoma cells. Cancer Biol Ther. 2018; 19: 786–96. [PubMed: 30024813]
49. Montano R, Thompson R, Chung I, Hou H, Khan N, Eastman A. Sensitization of human cancer cells to gemcitabine by the Chk1 inhibitor MK-8776: cell cycle perturbation and impact of administration schedule in vitro and in vivo. BMC Cancer. 2013; 13: 604. [PubMed: 24359526]
50. Zhou ZR, Yang ZZ, Wang SJ, Zhang L, Luo JR, Feng Y, et al. The Chk1 inhibitor MK-8776 increases the radiosensitivity of human triple-negative breast cancer by inhibiting autophagy. Acta Pharmacol Sin. 2017; 38: 513–23. [PubMed: 28042876]
51. Yamaguchi R, Perkins G, Hirota K. Targeting cholesterol with β-cyclodextrin sensitizes cancer cells for apoptosis. FEBS Lett. 2015; 589: 4097–105. [PubMed: 26606906]
52. Chou TC. Drug combination studies and their synergy quantification using the Chou-Talalay method. Cancer Res. 2010; 70: 440–6. [PubMed: 20068163]
53. BLISS CI. THE TOXICITY OF POISONS APPLIED JOINTLY1. Ann Appl Biol. 1939; 26: 585–615.
54. Hill SJ, Clark AP, Silver DP, Livingston DM. BRCA1 pathway function in basal-like breast cancer cells. Mol Cell Biol. 2014; 34: 3828–42. [PubMed: 25092866]
55. Ma X, Dang C, Min W, Diao Y, Hui W, Wang X, et al. Downregulation of APE1 potentiates breast cancer cells to olaparib by inhibiting PARP-1 expression. Breast Cancer Res Treat. 2019; 176: 109–17. [PubMed: 30989461]
56. Mladenova V, Russev G. DNA interstrand crosslinks repair in mammalian cells. Z Naturforsch C J Biosci. 2008; 63: 289–96. [PubMed: 18533476]
57. Fraser M, Zhao H, Luoto KR, Lundin C, Coackley C, Chan N, et al. PTEN deletion in prostate cancer cells does not associate with loss of RAD51 function: implications for radiotherapy and chemotherapy. Clin Cancer Res. 2012; 18: 1015–27. [PubMed: 22114138]
58. Zhang YW, Jones TL, Martin SE, Caplen NJ, Pommier Y. Implication of checkpoint kinase-dependent up-regulation of ribonucleotide reductase R2 in DNA damage response. J Biol Chem. 2009; 284: 18085–95. [PubMed: 19416980]
59. O'Flanagan CH, O'Shea S, Lyons A, Fogarty FM, McCabe N, Kennedy RD, et al. IGF-1R inhibition sensitizes breast cancer cells to ATM-related kinase (ATR) inhibitor and cisplatin. Oncotarget. 2016; 7: 56826–41. [PubMed: 27472395]
60. Speroni J, Federico MB, Mansilla SF, Soria G, Gottifredi V. Kinase-independent function of checkpoint kinase 1 (Chk1) in the replication of damaged DNA. Proc Natl Acad Sci U S A. 2012; 109: 7344–9. [PubMed: 22529391]

61. Sanjiv K, Hagenkort A, Calderon-Montano JM, Koolmeister T, Reaper PM, Mortusewicz O, et al. Cancer-Specific Synthetic Lethality between ATR and CHK1 Kinase Activities. Cell Rep. 2016; 17: 3407–16.

62. Gonzalez Besteiro MA, Calzetta NL, Loureiro SM, Habif M, Betous R, Pillaire MJ, et al. Chk1 loss creates replication barriers that compromise cell survival independently of excess origin firing. EMBO J. 2019; 38 e101284 [PubMed: 31294866]

63. Webster JA, Tibes R, Morris L, Blackford AL, Litzow M, Patnaik M, et al. Randomized phase II trial of cytosine arabinoside with and without the CHK1 inhibitor MK-8776 in relapsed and refractory acute myeloid leukemia. Leuk Res. 2017; 61: 108–16. [PubMed: 28957699]

64. Sen T, Della Corte CM, Milutinovic S, Cardnell RJ, Diao L, Ramkumar K, et al. Combination Treatment of the Oral CHK1 Inhibitor, SRA737, and Low-Dose Gemcitabine Enhances the Effect of Programmed Death Ligand 1 Blockade by Modulating the Immune Microenvironment in SCLC. J Thorac Oncol. 2019; 14: 2152–63. [PubMed: 31470128]

65. Brideau C, Gunter B, Pikounis B, Liaw A. Improved statistical methods for hit selection in high-throughput screening. J Biomol Screen. 2003; 8: 634–47. [PubMed: 14711389]

66. Bohula EA, Salisbury AJ, Sohail M, Playford MP, Riedemann J, Southern EM, et al. The efficacy of small interfering RNAs targeted to the type 1 insulin-like growth factor receptor (IGF1R) is influenced by secondary structure in the IGF1R transcript. J Biol Chem. 2003; 278: 15991–7. [PubMed: 12604614]

Europe PMC Funders Author Manuscripts

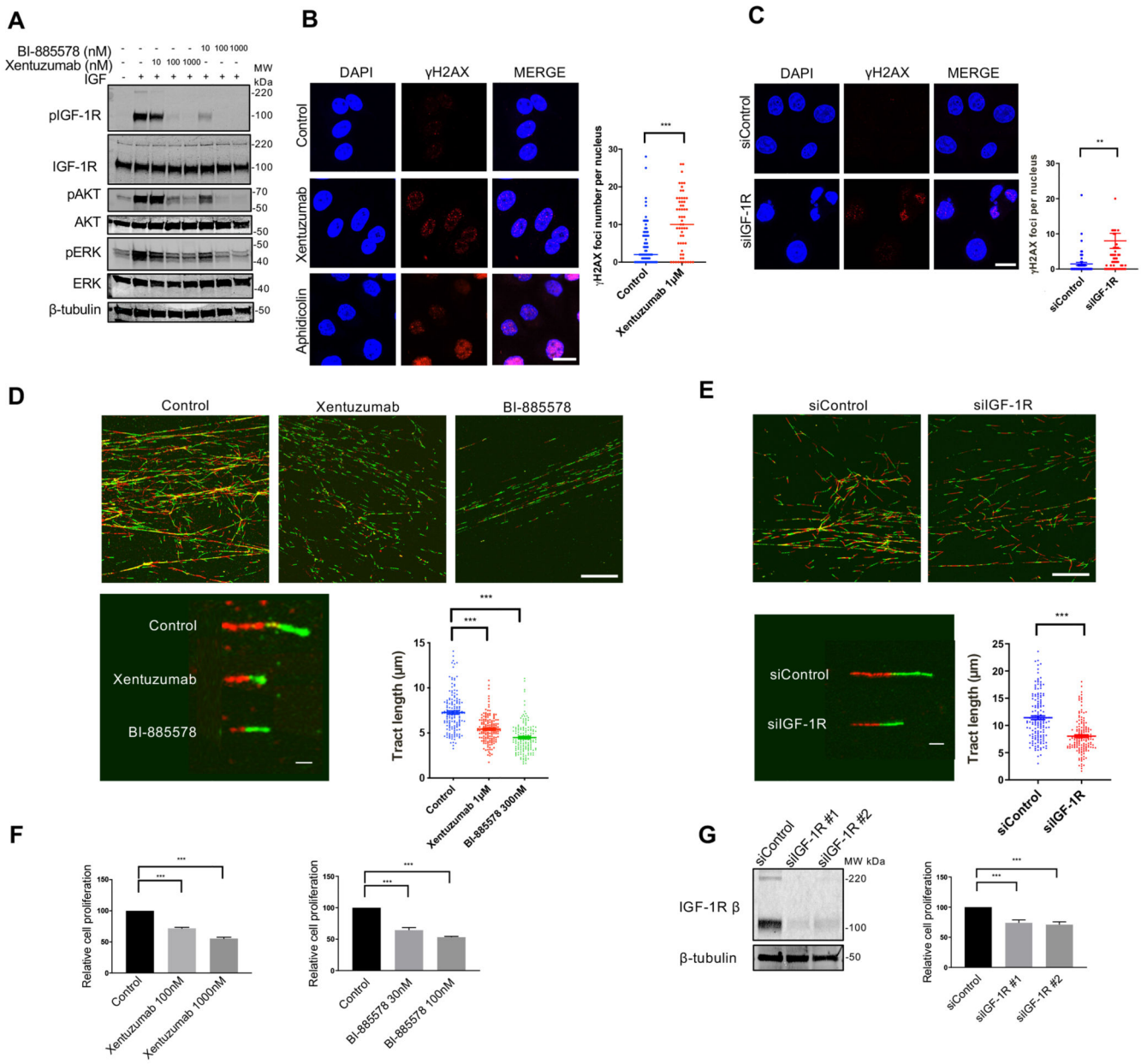

Figure 1. IGF blockade induces tolerable replication stress

(A) Western blot analysis of MCF7 cells exposed to xentuzumab or BI-885578 for 4 days, serum starved for 24 hours in the presence of the same inhibitors and stimulated with 50 nM IGF-1 for 15 minutes. **(B)** Representative image of γH2AX immunostaining in MCF7 cells treated with 1 μM xentuzumab or 0.3 μM aphidicolin for 72 hours. Scale bar: 20 μm. Graph to right: quantification of γH2AX (>50 cells). Data represent mean ± SEM, pooled from 3 independent experiments. **(C)** Representative image of γH2AX immunostaining in MCF7 cells transfected with siControl or siIGF-1R for 48 hours. Scale bar: 20 μm. Graph to right: quantification of γH2AX (>50 cells per condition). **(D)** Representative images of DNA fiber tracts (CIdU, red; IdU, green) in MCF7 treated with xentuzumab (1 μM) or BI-885578 (300nM) for 24 hours. Scale bar: 20 μm. Graph to right: quantification of fiber tract length

(>150 tracts) analysed using ImageJ software. **(E)** Representative images of DNA fibers in MCF7 cells transfected with siControl or siIGF-1R for 48 hours. Scale bar: 20 μm. Quantification of fiber tract length (>150 tracts) shown on the right. **(F)** Cell viability tested 5 days after drug treatment (CellTiter Blue assay) expressed as % viability of solvent-treated controls. **(G)** Western blot analysis of MCF7 cells transfected with siControl or siIGF-1R and lysed after 24 hours (Left). Transfected cells were collected 24 hour later and reseeded for cell viability assay (5 days after 24 hours transfection). Results were expressed as % viability of siControl-transfected cells (right). *P < 0.05, **P < 0.01, ***P < 0.001.

Europe PMC Funders Author Manuscripts

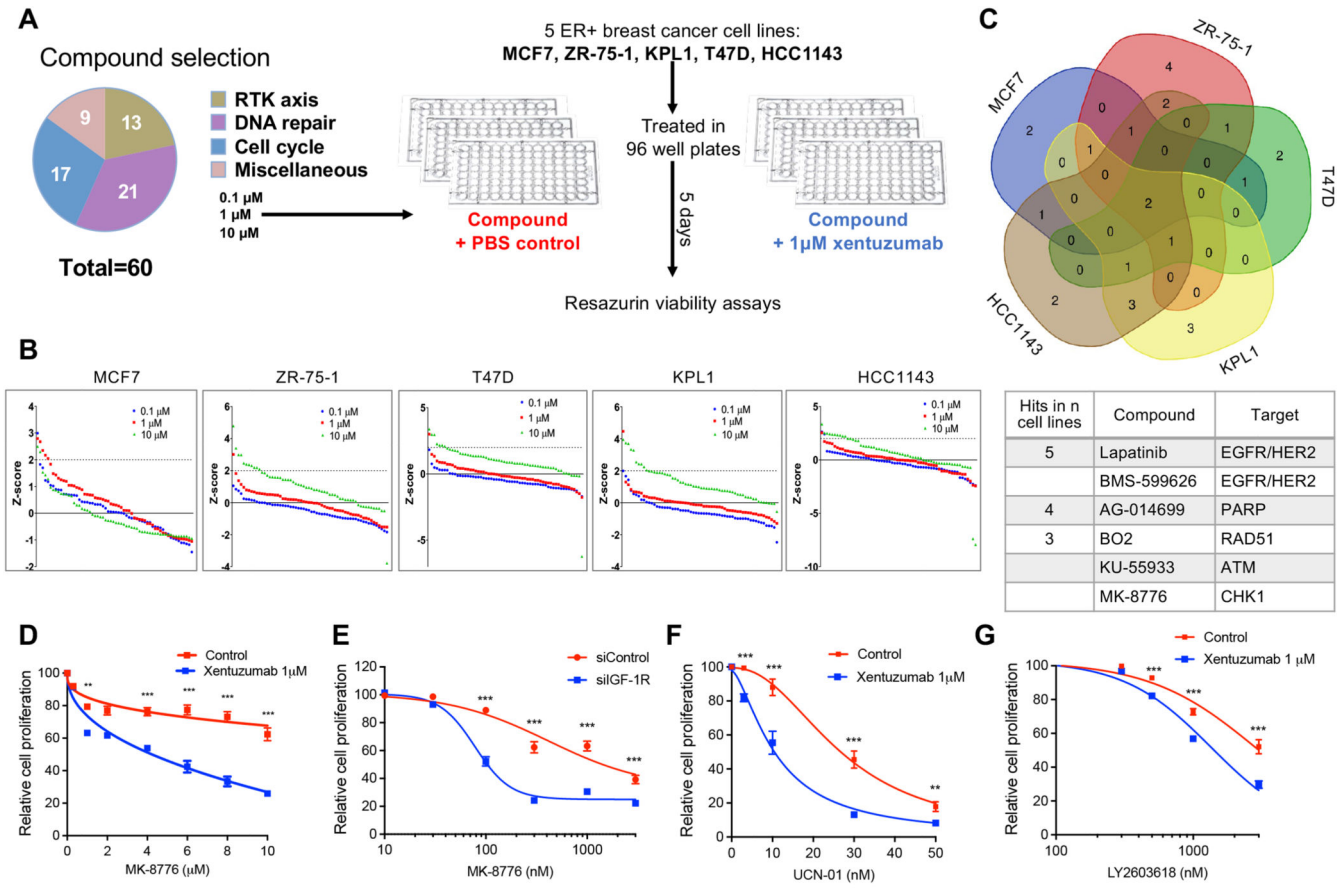

Figure 2. Compound screen identifies drug combination of CHK1 inhibitor and IGF inhibitor

(A) Compound library contained 59 small molecule drugs and controls (DMSO solvent for compounds, PBS for xentuzumab). MCF7, ZR-75-1, KPL1, T47D, HCC1143 were seeded in 96-well plates, treated with DMSO or library compounds at 0.1 μM, 1 μM, 10 μM with PBS or 1 μM xentuzumab and cell viability was determined after 5 days. **(B)** Cell viability data were used to calculate Z-scores as described in Supplementary Methods. Z-scores were ranked for all compounds for each cell line. Dotted line: Z-score=2, threshold for hit identification. **(C)** Venn diagram showing overlap of hit compounds in 5 cell lines. Below: screen hits in at least 3 cell lines. **(D)** MCF7 cells were exposed to xentuzumab and MK-8776 for 5 days. **(E)** MCF7 cells were transfected with siControl or siIGF-1R for 24 hours, and then exposed to solvent (control) or MK-8776 for 5 days. **(F-G)** MCF7 cells were exposed for 5 days to xentuzumab with UCN-01 (F) or LY2603618 (G) prior to cell viability assay. Data in D-G were expressed as % viability of solvent-treated control or siControl cells and represent mean ± SEM, pooled from n=3 independent experiments. Two-way ANOVA of data in D-G indicated that both xentuzumab and IGF-1R depletion induced significant difference ($P<0.001$) in the response to CHK1 inhibition; graphs show post-hoc analysis of significance at each drug concentration.

Europe PMC Funders Author Manuscripts

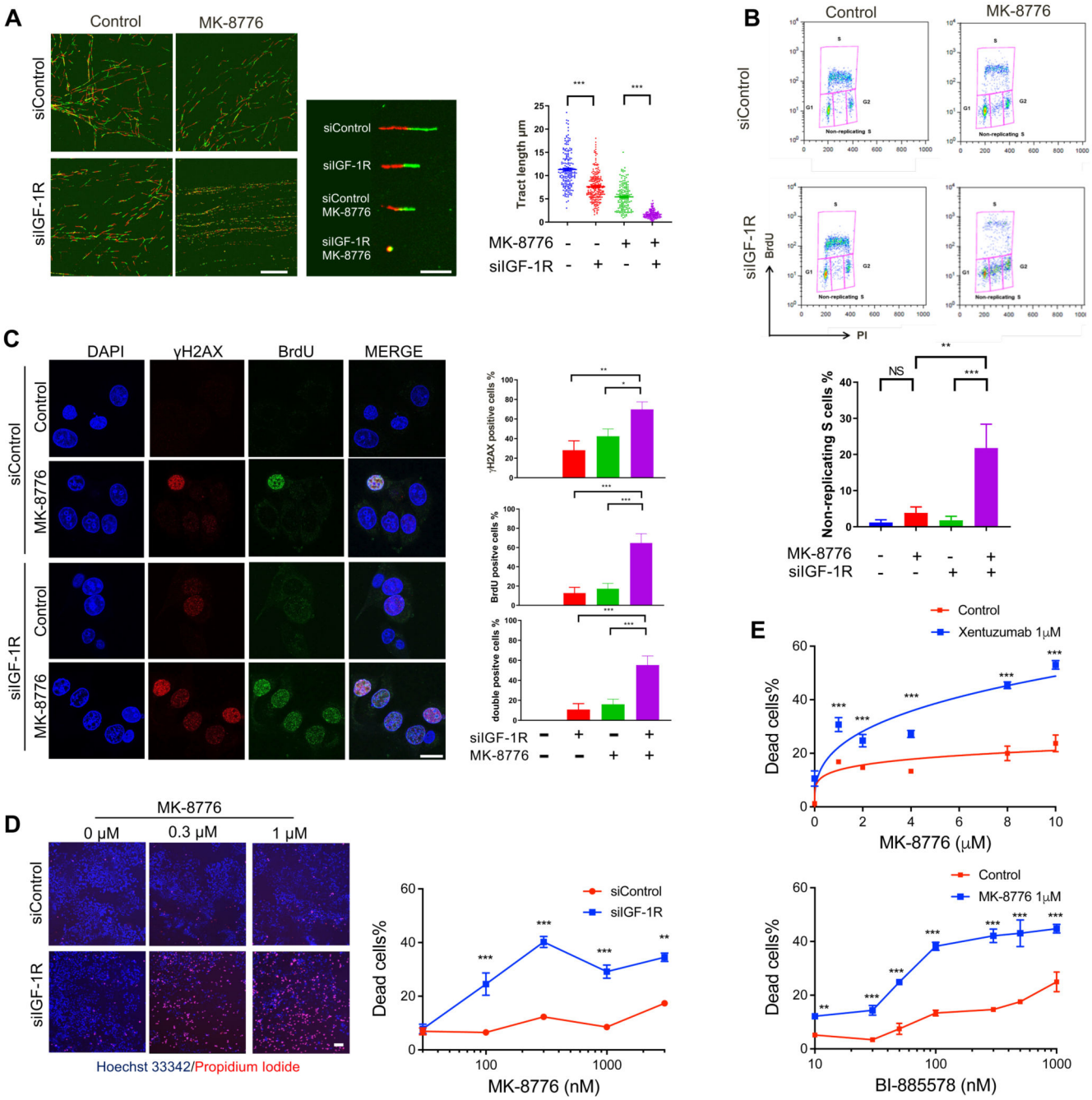

Figure 3. CHK1 inhibition induces replication catastrophe in IGF-1R depleted cells

(A) Representative images of DNA fiber tracts in MCF7 cells transfected with siControl or siIGF-1R for 24 hours and then exposed to solvent or 300 nM MK-8776 for 24 hours. Scale bar: 20 µm. Graph: quantification of fiber tract length (>150 tracts). **(B)** Flow cytometry analysis of cell cycle distribution of MCF7 cells after siRNA transfection for 24 hours and then exposure to solvent or 300 nM MK-8776 for 24 hours. Quantification of non-replicating S phase cells is represented as mean ± SD, pooled from 3 independent experiments. These data were gated to exclude cells with >4N DNA content; ungated data

Europe PMC Funders Author Manuscripts

Europe PMC Funders Author Manuscripts

are shown in Supplementary Figure S3E. **(C)** Representative images of BrdU and γH2AX immunofluorescence in MCF7 cells transfected with siControl or siIGF-1R for 24 hours and then exposed to solvent or 300 nM MK-8776 for 24 hours. Cells were cultured with 10 μM BrdU for 36 hours before fixation and analysed in non-denaturing conditions to detect ssDNA. Scale bar: 20 μm. Graphs to right: upper, γH2AX positive cells (>10 foci + pan-nuclear staining); centre, BrdU positive cells (>5 foci + pan-nuclear staining); lower, double-positive cells; ≥10 images were quantified. **(D)** Representative images of PI/Hoechst 33342 staining in MCF7 cells transfected with siControl or siIGF-1R for 24 hours and then exposed to solvent or MK-8776 for 5 days. Scale bar: 200 μm. Graph below: dead cells % expressed as % PI positive cells/Hoechst positive cells. Data represent mean ± SEM, pooled from 3 independent experiments. **(E)** MCF7 cells were exposed to xentuzumab (upper) or BI-885578 (lower) in combination with solvent or MK-8776 for 5 days. Dead cells expressed as mean ± SEM % PI positive cells/Hoechst positive cells. For D-E there was a significant difference between each of the dose-response curves ($P<0.001$) by 2-way ANOVA.

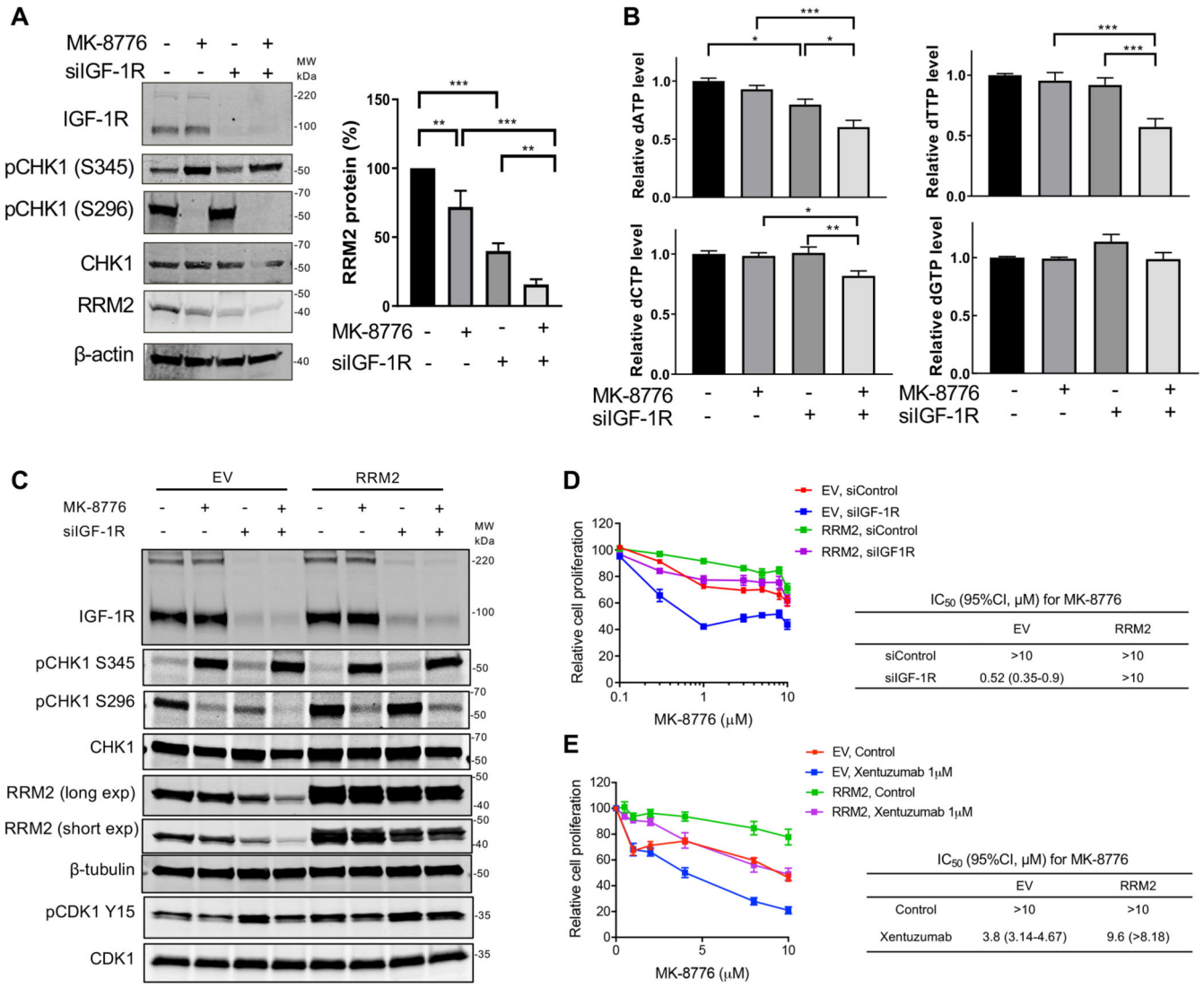

Figure 4. CHK1 inhibition reduces RRM2 protein levels and decreases dNTP pools in IGF-1R depleted cells

(A) Western blot analysis of MCF7 cells transfected with siControl or siIGF-1R for 24 hours, and exposed to solvent or 300 nM MK-8776 for 24 hours. Graph: RRM2 protein levels were quantified by ImageJ, corrected for β-tubulin loading and expressed as percent RRM2 protein content of solvent-treated controls. Data represent mean ± SEM from 3 independent experiments. **(B)** dNTPs extracted from cells in A) were assayed, results were normalised to solvent controls (left bar) and represent mean ± SEM, pooled from 3 independent experiments. **(C)** Empty vector (EV) control cells and RRM2-overexpressing cells were transfected with siControl or siIGF-1R for 24 hours and then exposed to solvent or 300nM MK-8776 for 24 hours, followed by protein extraction and western blot analysis. **(D)** EV controls and RRM2-overexpressing cells were siRNA transfected as C and then exposed to solvent or MK-8776 for 5 days, followed by cell viability assay. Results were expressed as % viability of solvent-treated control. IC_{50} values and 95% confidence intervals (CI) were calculated from dose-response curves. By 2-way ANOVA there were

Europe PMC Funders Author Manuscripts

significant differences in response to MK-8776 in siControl vs siIGF-1R transfected EV cells, siControl vs siIGF-1R transfected RRM2-overexpressing cells and siControl EV cells vs siControl RRM2 transfectants ($P<0.001$ for each comparison) but no significant difference in siControl EV cells vs siIGF-1R transfected RRM2-overexpressing cells. **(E)** EV control cells and RRM2-overexpressing cells were exposed to solvent or MK-8776 in the presence or absence of 1 μM xentuzumab for 5 days followed by assay of cell viability, expressed as % of solvent-treated controls, showing IC_{50} values and 95% CI. Two-way ANOVA showed significant differences in response to MK-8776 in solvent controls vs xentuzumab-treated EV cells, controls vs xentuzumab-treated RRM2-overexpressing cells and control-treated EV vs RRM2-overexpressing cells ($P<0.001$ for each comparison) and no significant difference in the response of control-treated EV cells vs xentuzumab-treated RRM2-overexpressing cells.

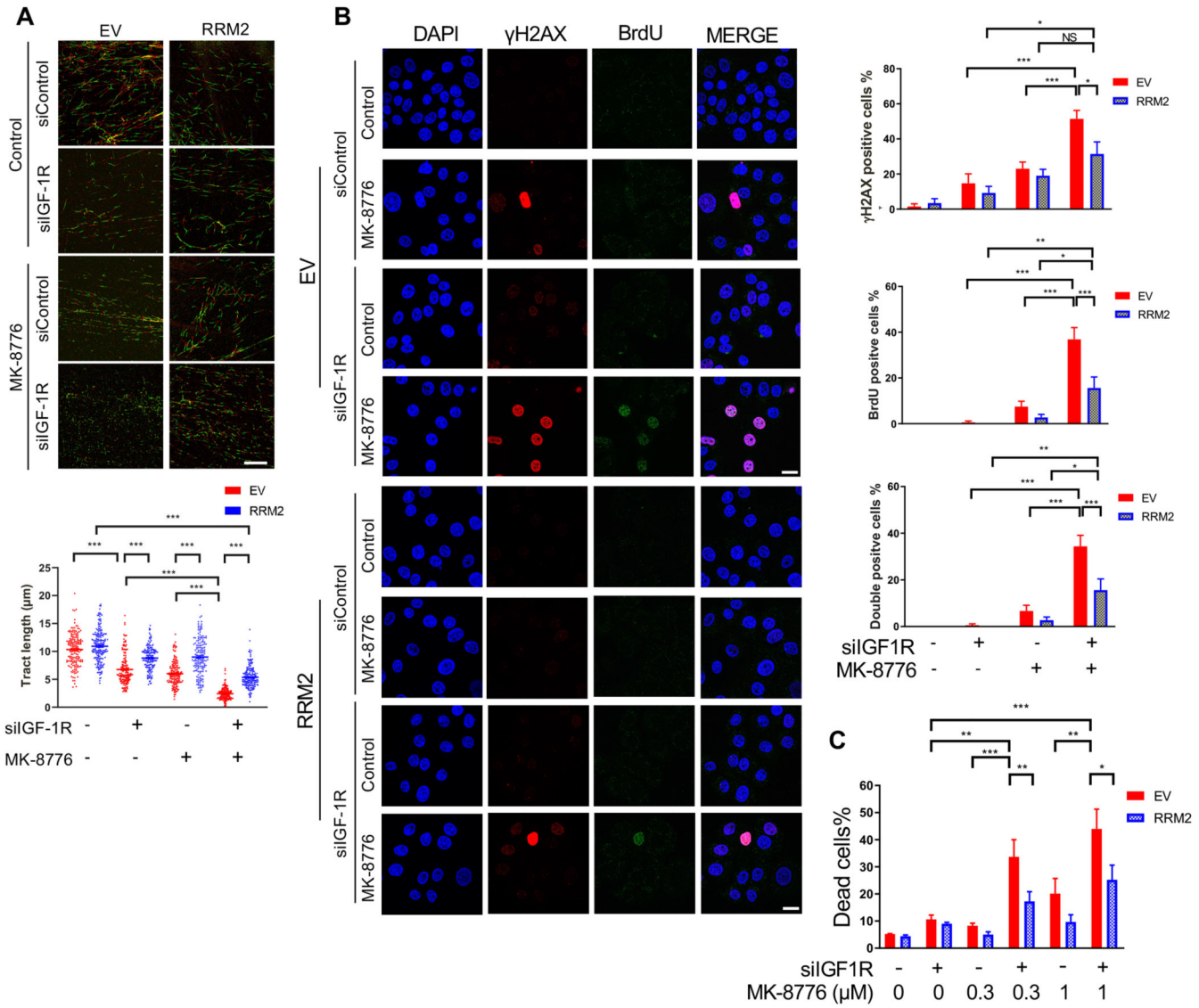

Figure 5. RRM2 overexpression rescues replication catastrophe induced by CHK1 inhibition and IGF-1R depletion

(A) Representative images of DNA fiber tracts in EV controls and RRM2-overexpressing cells transfected with siControl or siIGF-1R for 24 hours and exposed to solvent or 1 μM MK-8776 for 24 hours. Scale bar: 20 μm. Graph below: quantification of fiber tract length (>150 tracts). **(B)** Representative images of BrdU and γH2AX immunostaining in EV control cells and RRM2-overexpressing cells siRNA transfected and treated as A, with addition of 10 μM BrdU for 36 hours before fixation and analysis in non-denaturing conditions. Scale bar: 20 μm. Graphs to right: quantification of γH2AX positive, BrdU positive and double positive cells as in Figure 3C; data represent mean ± SEM, pooled from 3 independent experiments. **(C)** EV controls and RRM2-overexpressing cells were transfected with siControl or siIGF-1R for 24 hours and then exposed to solvent control or MK-8776 for 5 days, followed by PI/Hoechst 33342 staining to quantify dead cells,

Europe PMC Funders Author Manuscripts

expressed as % PI-positive/Hoechst positive cells. Data represent mean ± SEM, pooled from 3 independent experiments each with 3 technical replicates.

Europe PMC Funders Author Manuscripts

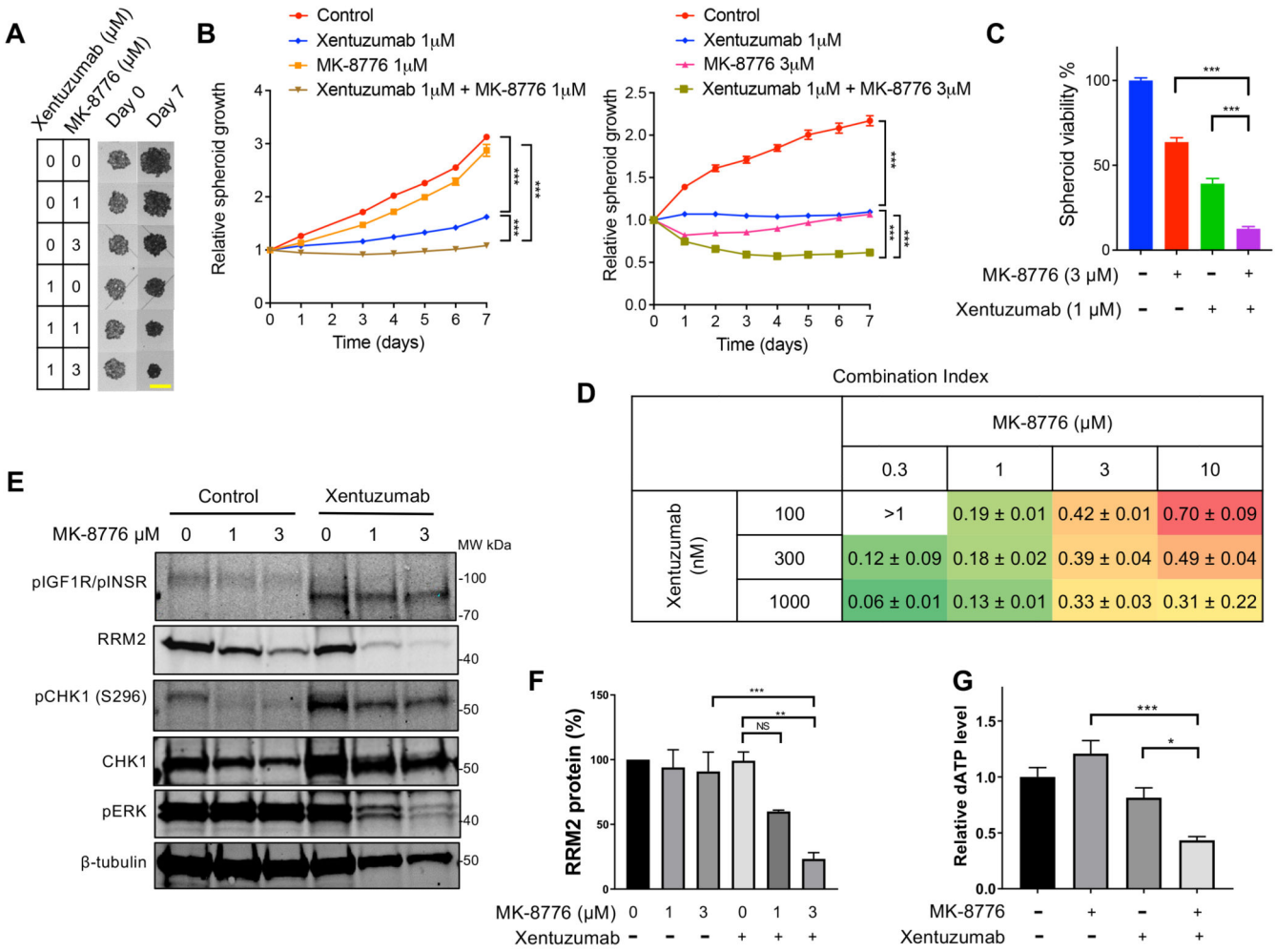

Figure 6. IGF inhibited cells are sensitive to CHK1 inhibition in 3D spheroid models

(A) Representative images of SK-CO-1 spheroids exposed to xentuzumab alone or with MK-8776 for 7 days. Scale bar 2 mm. **(B)** Spheroid growth curves shown as fraction of Day 0 (pre-treatment) value. Two-way ANOVA showed a significant overall treatment effect and significantly reduced growth rates between xentuzumab or 1 or 3 μM MK-8776 alone and in combination ($P<0.001$ for each comparison). **(C)** After 7 days, on completion of treatments and measurements in A-B, CellTiter Glo 3D viability assays were performed, and results expressed as mean ± SEM % solvent-treated controls pooled from n=3 independent experiments. **(D)** CellTiter Glo 3D viability data were imported into CalcuSyn Software for CI value calculation. Data represent mean ± SD, pooled from 3 independent experiments. **(E)** Western blot analysis of SK-CO-1 spheroids (6 spheroids per condition) exposed to solvent or MK-8776 in the presence or absence of 1 μM xentuzumab for 7 days. **(F)** RRM2 protein levels were quantified and adjusted for β-tubulin loading. Graph shows mean ± SEM RRM2 protein from 3 independent experiments, expressed as % of solvent-treated controls. **(G)** SK-CO-1 spheroids were treated with 1 μM xentuzumab and/or 3 μM MK-8776. Spheroid extracts were assayed for dATP and the results were normalised to solvent controls (left bar). Data represent mean ± SEM, pooled from 3 independent experiments.

Europe PMC Funders Author Manuscripts

Europe PMC Funders Author Manuscripts

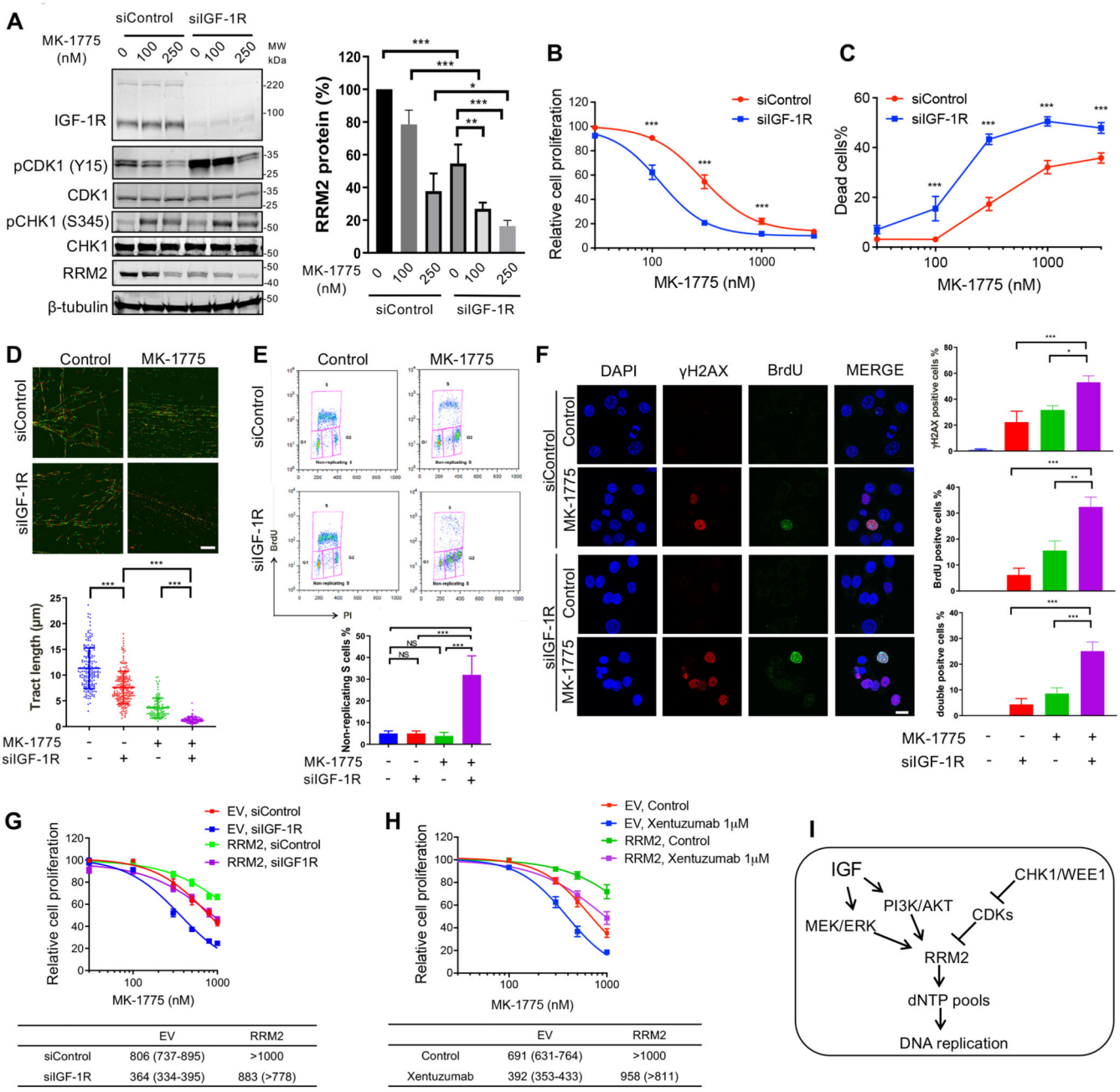

	EV	RRM2
siControl	806 (737-895)	>1000
siIGF-1R	364 (334-395)	883 (>778)

	EV	RRM2
Control	691 (631-764)	>1000
Xentuzumab	392 (353-433)	958 (>811)

Figure 7. WEE1 inhibition induces replication catastrophe in IGF-1R depleted cells

(A) Western blot of MCF7 cells transfected with siControl or siIGF-1R for 24 hours and exposed to solvent or MK-1775 for 24 hours. Graph: RRM2 protein levels were quantified by ImageJ, corrected for β-tubulin and shown as mean ± SEM % of solvent-treated controls from 3 independent western blots. **(B, C)** MCF7 cells were transfected with siControl or siIGF-1R for 24 hours and treated with solvent or MK-1775 for 5 days, followed by cell viability assay (B) or cell death assay (C), with significant differences (P<0.001) in response to MK-1775 in both assays by 2-way ANOVA. **(D)** Representative images of DNA fiber tracts in MCF7 cells transfected with siControl or siIGF-1R for 24 hours

Europe PMC Funders Author Manuscripts

and exposed to solvent or 300 nM MK-1775 for 24 hours. Scale bar: 20 μm. Graph below: quantification of fiber tract length (mean ± SEM of >150 tracts). **(E)** Analysis of MCF7 cell cycle distribution after transfection with siControl or siIGF-1R for 24 hours and exposed to solvent or 300 nM MK-1775 for 24 hours. Graph below shows quantification of non-replicating S phase cells, mean ± SD, pooled from 3 independent experiments. **(F)** Representative images of native BrdU and γH2AX immunostaining in MCF7 cells transfected and treated as E, and cultured with 10 μM BrdU for 36 hours pre-fixation. Scale bar: 20 μm. Graphs to right: quantification of γH2AX positive, BrdU positive and double positive cells as Figure 3C; data represent mean ± SEM, pooled from 3 independent experiments. **(G)** EV controls and RRM2-overexpressing cells were transfected with siControl or siIGF-1R for 24 hours, exposed to solvent or MK-1775 for 5 days, and cell viability was assayed. Data represent mean ± SEM, pooled from n=3 independent experiments; below: IC_{50} values and 95% CI calculated from drug response curves. Two-way ANOVA showed similar differences in response to MK-1775 as in response to MK-8776 (Figure 4D-E), with significant differences in siControl vs siIGF-1R transfected EV cells, siControl vs siIGF-1R transfected RRM2-overexpressing cells and siControl EV cells vs siControl RRM2 transfectants ($P<0.001$ for each comparison) but not in siControl EV cells vs siIGF-1R transfected RRM2-overexpressing cells. **(H)** EV controls and RRM2-overexpressing cells were exposed to solvent or MK-1775 in the presence or absence of 1 μM xentuzumab for 5 days, followed by cell viability assay. Data represent mean ± SEM, pooled from n=3 independent experiments with below, GI_{50} values and 95% CI. There were significant differences in response to MK-1775 in solvent controls vs xentuzumab-treated EV cells, controls vs xentuzumab-treated RRM2-overexpressing cells and control-treated EV vs RRM2-overexpressing cells ($P<0.001$ in each case) but not in control-treated EV cells vs xentuzumab-treated RRM2-overexpressing cells. **(I)** RRM2 is regulated by IGFs and cell cycle checkpoint kinases CHK1 and WEE1, explaining profound RRM2 downregulation and replication catastrophe upon IGF:CHK1 or IGF:WEE1 co-inhibition.